A Segmentation Method for Intracoronary Optical Coherence Tomography (OCT) Image Based on Least Squares Support Vector Machine: Vulnerable Coronary Plaque Cap Thickness Quantification

†Xiaoya Guo,[1] Dalin Tang,[1*,2] David Molony, [3] Chun Yang,[2] Habib Samady[3], Jie Zheng[4], Gary S. Mintz[5], Akiko Maehara[5], Liang Wang[2], Xuan Pei[6], Zhi-Yong Li[6], Genshan Ma[7*], Don P. Giddens[3,8]

[1] Department of Mathematics, Southeast University, Nanjing, 210096, China
[2] Mathematical Sciences Department, Worcester Polytechnic Institute, Worcester, MA 01609 USA
[3] Department of Medicine, Emory University School of Medicine, Atlanta, GA, 30307, USA
[4] Mallinckrodt Institute of Radiology, Washington University, St. Louis, MO, 63110, USA
[5] The Cardiovascular Research Foundation, Columbia University, New York, NY 10022, USA
[6] School of Biological Science & Medical Engineering, Southeast University, Nanjing, China
[7] Department of Cardiology, Zhongda Hospital, Southeast University Nanjing, 210009, China
[8] The Wallace H. Coulter Department of Biomedical Engineering, Georgia Institute of Technology, Atlanta, GA, 30332 USA

† Presenting author: Xiaoya Guo, Southeast University, Nanjing China;
* Corresponding authors: Dalin Tang, Southeast University, Nanjing China, email: dtang@wpi.edu, fax number: 508 831-5824; Genshan Ma, Southeast University, Nanjing China, magenshan@hotmail.com.

Abstract

Accurate cap thickness quantification is of fundamental importance for vulnerable plaque research. A segmentation method for intracoronary optical coherence tomography (OCT) image based on least squares support vector machine (LS-SVM) to characterize plaque lumen surface, segment borders and fibrous cap for plaque cap thickness when image quality is not high enough, especially at the location of bifurcation.

In vivo intravascular ultrasound (IVUS) and OCT coronary plaque data were acquired from one patient with informed consent obtained. Manual segmentation in OCT images based on the combination of VH-IVUS image and OCT image were given by experts as the gold standard. Processed OCT images were trained and tested via LS-SVM by two methods (M1 and M2). In M1, 500 pixels were randomly selected from each lipid class and vessel tissue class for 9 OCT images. The training data set would be the feature vectors from 9000 pixels. In M2, a procedure similar to leave-one-out cross validation was employed as any 8 out of 9 images were used as training data while the remaining one as the testing data. Borders and lipid contours were extracted from prediction results for cap thickness. Virtual histology (VH) IVUS data were processed with minimum cap thickness set as 50 and 180 micron to generate IVUS50 and IVUS180 data sets, respectively. Cap thickness from manual segmentation, predictions from M1 and M2 based LS-SVM, IVUS50 and IVUS180 data sets were compared.

The accuracy of M1 and M2 were above 76%. Average of mean cap thickness (unit: mm) from 9 images was 0.561 (manual), 0.470 (M1), 0.463 (M2), 0.128 (IVUS50) and 0.204 (IVUS180). Average of minimum cap thickness (9 slices) was 0.390 (manual), 0.288 (M1), 0.282 (M2), 0.040 (IVUS50) and 0.165 (IVUS180). IVUS50 and IVUS180 underestimated cap thickness. The mean cap thickness from prediction were close to manual results (error<18%). The point-point cap thickness from five groups showed that the prediction based LS-SVM had agreement with manual segmentation.

Conclusion. The segmentation methods based on LS-SVM provided reasonable accuracy for plaque cap thickness quantification. More data sets and better gold standard are needed for further improvement.

Keywords: Vulnerable plaque; coronary; OCT; cap thickness; LS-SVM; segmentation.

1. Introduction

Coronary atherosclerotic plaques often rupture without warning and cause acute syndromes, such as heart attack. It is commonly believed that atherosclerotic plaques rupture is closely associated with thin fibrous cap (cap thickness < 65 μm) which covers a large lipid-rich necrotic core [1-2]. Advanced medical imaging technologies have been employed to identify the plaque morphology. Intravascular ultrasound (IVUS) is one of the major imaging tools to visualize coronary plaques, and is also extensively used for constructing computational coronary models. Virtual histology IVUS (VH-IVUS) segments the grayscale IVUS data into four tissue types: fibrotic, fibro-fatty, lipid necrotic core and dense calcified tissue [3-5]. Although VH-IVUS has provided unique perspectives on in vivo human atherosclerotic plaque and novel insights into plaque morphology and natural history, it still has limited resolution of 150-250 micron and is not able to detect thin plaque cap with thickness around 65 μm, the critical threshold value determined from histopathological studies [1, 6]. Quantifying cap thickness and its impact on stress/strain calculations remains to be a great challenge for plaque research.

In recent years, optical coherence tomography (OCT) has emerged as an imaging modality to identify vulnerable plaques from non-vulnerable plaques to enhance future risk prediction. This medical imaging technology provides a resolution of approximately 10 μm which is far better than what IVUS could achieve. OCT has the capacity of characterizing the superficial structure of the vessel in greater detail [7-8]. Traditionally, the segmentation of OCT images to detect lumen and plaque components has been performed manually [9-10]. Rabel et al. introduced a manual method combined IVUS/VH-IVUS and OCT images to characterize the plaque [11]. The combination of IVUS/VH-IVUS and OCT images provided more complete plaque information. However, Manual segmentation is a time-consuming procedure and it also suffers higher inter- and intra-user variability. To overcome these limitations, some approaches for semi-automatic and fully-automatic segmentations have been proposed. Wang et al. introduced a semiautomatic segmentation of calcified plaques which is signal-poor regions with sharply delineated borders in OCT images [12]. Wang et al. provided semiautomatic segmentation using a dynamic programming algorithm to quantified fibrous cap [13]. The methodology using attenuation coefficients to characterize plaques [14-15]. Athanasiou developed an automated methodology for the segmentation of the composition of the superficial plaque in OCT images [16]. Some researchers used support vector machine (SVM) to classify plaque components [17-18]. Most methods in previous literatures aimed at segmenting high quality images. However, image quality is often affected by bifurcation, thrombus, and residual blood, etc. Necrotic core is signal-poor regions which have poor diffuse borders in OCT images. Accurate detection of lipid-rich necrotic core (lipid in short) is still a challenging task.

While OCT has high resolution and can quantify thin cap thickness, it has limited penetration (1 to 2 mm) and is often unable to provide complete information of the whole vessel, especially at the

locations with large lumen, bifurcation and increased plaque burden [7]. In this paper, we introduced an OCT segmentation method to characterize plaque lumen surface, segment borders and fibrous cap for plaque cap thickness when image quality is not high enough, especially at the location of bifurcation. Support vector machine was used in separating lipid component and vessel tissue. Validation was performed based on the segmented results from experts on VH-IVUS and OCT images.

2. Data and Methods

2.1 Data acquisition

In vivo OCT data were acquired from one patient (male, age 51) using ILUMIEN OPTIS System, and Dragonfly JP Imaging Catheter (St. Jude, Minnesota, MN) with informed consent obtained. During image acquisition, blood was displaces by the injection of Dextran, and the OCT catheter was traversed to the region of interest an automatic pullback at 20mm/s was performed. OCT raw data were logarithmically compressed grayscale images with pixel intensity recorded as a two-dimensional matrix in polar coordinates $I(r,\Theta)$, where r is the range dimension and Θ is the acquisition angle. The OCT image in polar coordinate $I(r,\Theta)$ was converted to Cartesian coordinates I(i,j) for later image processing, using the relations: $i = r \cos \Theta$, $j = r \sin \Theta$. OCT images in Cartesian coordinates consists of 1024 by 1024 pixels representing a real physical size of 10mm by 10mm (pixel size: 9.9 by 9.9 micron).

IVUS images were recorded for the same segment of coronary using a 20MHz, 2.9F phased-array catheter (Eagle Eye Gold, Volcano Therapeutics, Rancho Cordova, CA). Following the OCT image acquisition, the IVUS catheter was traversed distally though the artery to the region of interest at an automatic pullback speed of 0.5mm/s. VH-IVUS images were created based on IVUS images by using autoregressive models to differentiate four plaque types: fibrous, fibro-fatty, necrotic core (lipid) and dense calcified tissue (calcification, Ca in short). Each plaque type is indicated by different color on the IVUS-VH image. The positions of both catheters were recorded with angiography for the co-registration of OCT and IVUS images. All imaging data were digitally stored for offline analysis.

Nine OCT images were selected from OCT data set of this patient with co-registered VH-IVUS images. Images from the locations of bifurcation were also considered in this paper. Tiny calcium was neglected in OCT images since fibrous cap was our main interested region. Experts provided manual lipid contours in OCT images based on the combination of VH-IVUS and OCT images following the standard procedure described in [11]. The manual lipid delineation was considered as the standard of classification and saved as image masks for comparison with our segmentation. Figure 1 shows VH-IVUS and OCT images as well as manually segmented lipid and lumen contours.

(a) VH-IVUS Slices

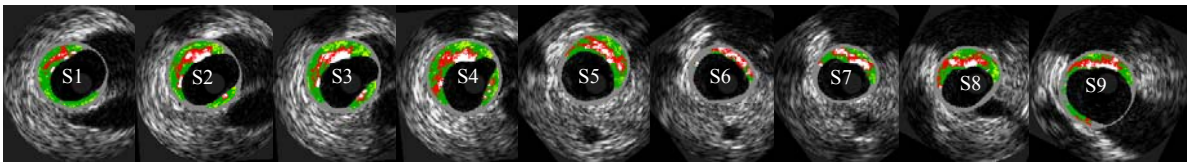

(b) Matching OCT Slices and Segmented Contours

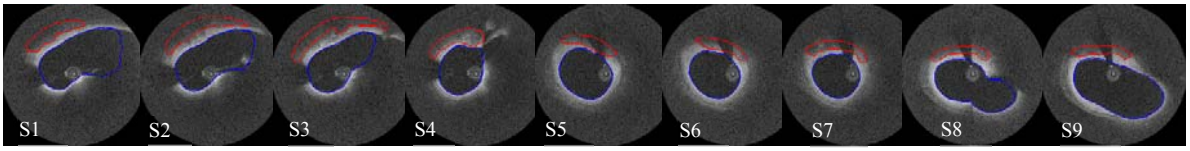

(c) Manual Segmented Contours

Figure 1. Nine matching VH-IVUS and OCT images and manual segmented contours. (a) Nine VH-IVUS slices; (b) Nine matching OCT images with the segmented contours; (c) Manual segmented contours combined OCT and VH-IVUS. Colors used in VH-IVUS: *Red* necrotic core, *White* dense calcium, *Dark Green* Fibrous, *Light Green* Fibro-Fatty.

2.2 Image processing

OCT images in polar coordinate were processing to detect lumen border by applying the following steps: filter, Otsu's thresholding method and removal of catheter and artifacts. More details of automatic lumen detection were given in [19-20]. Since fibrous cap thickness was an important focus in this study, the lumen border was expanded from center of catheter outward 1mm as the outer border to include enough space for fibrous cap characterization. At the locations of bifurcation, branches of the coronary without catheter passing through were removed along with its reduced artifacts. Thus the region of interest (ROI) was determined as the area bounded by lumen and outer border with artery branches and other artifacts removed. The detection of borders and the determination of ROI were showed in Figure 2.

(a) Region of interest

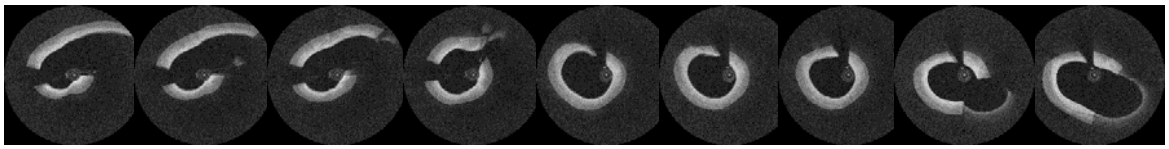

(b) Borders of ROI

Figure 2. Nine OCT images with ROI and borders of ROI. (a) ROI in OCT images. White color means ROI. (b) Borders of ROI.

2.3 Feature extraction and selection

Local binary patterns (LBPs), Gray level co-occurrence matrices (GLCMs), entropy and mean value were calculated as features in this work. All features were computed in an 11 by 11 pixels

neighborhood window in ROI. The window size had been tested to be the best in [16]. Gray level co-occurrence matrices (GLCMs) are a well-known method for texture analysis and 32 statistical features were extracted from GLCMs which were contrast, correlation, energy and homogeneity features for each of eight angles (Θ= 0, 45, 90, 135,180, 225, 270, 315 degree). LBPs is an image operator used to describe the local texture feature with rotating invariance and grayscale invariance. Rotation invariant LBPs with P=8, R=1 was used to extract ten features. Details and parameters can be found from [16, 21].

Superabundant features would affect the classification accuracy of classifier. Twenty-eight features were selected to improve the accuracy which contains 16 GLCMs (The four aforementioned features at each angle Θ= 0, 45, 90, 135 degree), 10 LBPs, entropy and mean value. These 28 features were the optimal feature combination to reach the highest accuracy for our classification algorithm based on this patient OCT images.

2.4 Classification

The data base to feed support vector machine (SVM) were assembled by all selected features extracted from all pixels in ROI into a data matrix with dimension n by m, where n is equal to the number of pixels and m is the length of the feature vector, more specifically 28 features in this work. Since fibrous cap could be identified once the lipid area is determined, only two classes are needed to be characterized indicating two different tissue types: lipid and vessel tissue. Since the recognitions of fibrous tissue and fibro-fatty tissue have no impact on the measurement of fibrous cap, so they are considered as vessel tissue. SVM separates feature patterns for two classes by defining one hyperplane that maximizes the separating margin between two classes. Least squares support vector machine (LS-SVM) follows the structural risk minimization principle of kernel function as learning machine which is an improved the conventional SVM. LS-SVM classifier was chosen to classify the lipid and vessel tissue with Gaussian Radial Basis Function as the kernel function and steepest descent method for searching optimal parameters. More details about LS-SVM can be found in [22-23].

Two methods were proposed to select the training data set to fit SL-SVM classifier. In the first method (denoted as M1), 500 pixels were randomly selected from each lipid class and vessel tissue class for 9 OCT images. The training data set would be the feature vectors from 9000 pixels. The rest of non-selected pixels in ROI of each image would be treated as testing data set, The process was repeated ten times to stabilize the classification error estimation. While in the second method (denoted as M2), a procedure similar to leave-one-out cross validation was employed as any 8 out of 9 images were used as training data while the remaining one as the testing data. For each group of 8 OCT images, 500 pixels were random selected from lipid class and vessel tissue class each to give 8000 pixels. The testing set consists of all pixels in ROI of the rest one OCT image. Nine times training and testing were done in this method. Figure 3 showed nine images of prediction from LS-SVM after processing using M1 and M2.

(a) Prediction from M1 after processing

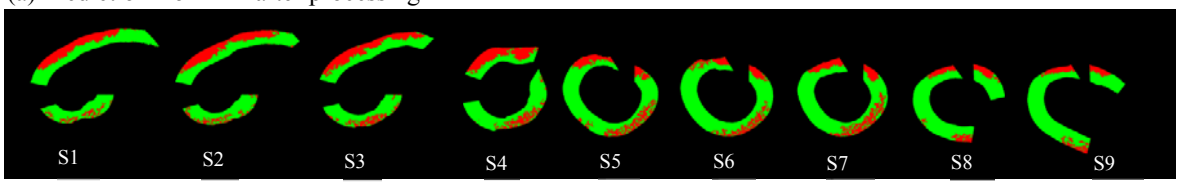

(b) Prediction from M2 after processing

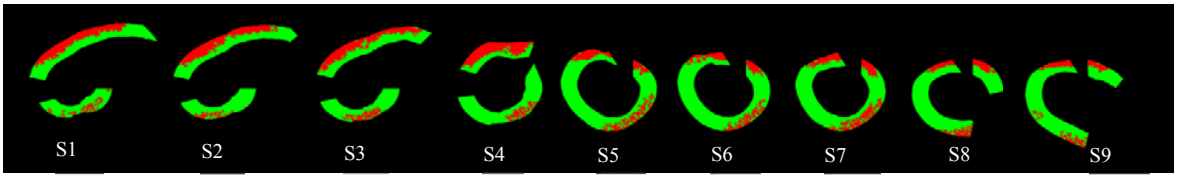

Figure 3. Prediction by LS-SVM from M1 and M2. (a) Prediction of 9 images from M1 after processing; (b) Prediction of 9 images from M2 after processing. Colors used in Prediction images: *Red* necrotic core, *Green* Fibrous and Fibro-Fatty.

2.5 Contours extraction

Lipid contours were extracted and its distance with lumen contour were calculated as cap thickness. The fibrous cap thickness was the greatest concern in this study, so lipid contours were extracted to quantify the cap thickness. According to the prediction of LS-SVM, the prediction images were processed to extract contours. Some scattered pixels in the images of prediction were filter to find the clear border in fibrous cap. Parametric active contour model was used for the lipid border detection. Figure 4 showed contours from active contour model.

(a) OCT contours from M1

(b) OCT contours from M2

Figure 4. Lipid contours and borders. Color contours: *Red* lipid contours, *Blue* borders.

2.6 Co-registered VH-IVUS segmentation

Cap thickness was the concerned part in this study. IVUS resolution limitation (150 μm), and original VH-IVUS data often had lipid core exposed directly to lumen, i.e., there is no fibrous cap covering the lipid core. A minimum cap thickness has to be added to VH-IVUS data so that the lipid cores would be covered. In our previous publications, 50 μm and 180 μm cap thickness were often added in VH-IVUS segmentation where 50 μm was chosen as it is a reasonable representative thin cap number < 65 μm threshold. VH-IVUS images were segmented by the custom-made software Atherosclerostic Plaque Segmentation software. In this work, minimum cap thickness value (50 μm and 180 μm) were set in our segmentation software. The segmented contours denoted as IVUS50 and IVUS180 (see Figure 5).

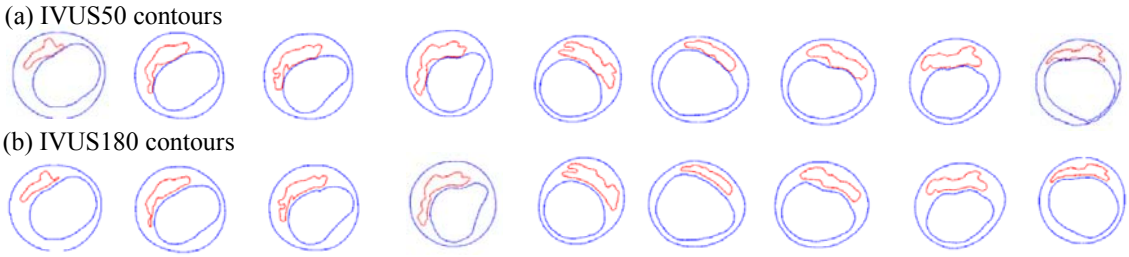

Figure 5. Segmented contours from IVUS50 and IVUS180. Color contours: *Red* lipid contours, *Blue* borders.

3. Results

3.1 Accuracy

The features data were used to train LS-SVM classifier which, in turn, would predict each data point in the testing data set into one of the classes (lipid and vessel-tissue) using the methods M1 and M2 described in Section 2.4. The prediction results was compared to manual segmentation to evaluate the prediction accuracy (denoted as Acc) defined as in the following formula:

$$Acc = \frac{TP+TN}{TP+FP+TN+FN} \tag{1}$$

Lipid and vessel tissue were set positive and negative pattern, respectively. Here TP is the number of true positive outcomes, FP is the number false positive outcomes, TN is the number of true negative outcomes and FN is the false negative outcomes. Sensitivity (Sen) and specificity (Spe) were also calculated using the formulas below to avoid the reliance of the uneven distributed data in two classes.

$$Sen = \frac{TP}{TP+FN} \tag{2}$$

$$Spe = \frac{TN}{TN+FP} \tag{3}$$

Table 1 gives the prediction results from ten times repeated experiment using M1. Table 1 gives the prediction results from ten times repeated experiment using M1. Sensitivity was about 10% higher than specificity for most OCT images. For the extreme worst case, sensitivity and specificity would still above 70%, while will achieve up to 97% for good cases during the ten times of trial. The average values of sensitivity and specificity are 89.6% and 78.6% respectively.

Table 2 compares the predictions accuracy of M1 and M2. Based on the average values of 9 OCT images, M1 showed a slightly better overall prediction accuracy than M2 (M1 (79.7%) vs M2 (76.1%)). For Sensitivity, M1 provided much higher value than M2 (M1 (89.6%) vs M2 (76.0%)) while the specificity values are quite close (M1 (78.6%) vs M2 (76.6%)). The good agreement between two methods demonstrated the stability of two automatic segmentation method proposed in this paper.

Table 1. Method 1 sensitivity and specificity from 10 tests.

Sensitivity	S1	S2	S3	S4	S5	S6	S7	S8	S9
T1	0.952	0.951	0.860	0.790	0.970	0.910	0.886	0.829	0.930
T2	0.940	0.930	0.851	0.791	0.974	0.922	0.905	0.851	0.927
T3	0.959	0.929	0.852	0.796	0.963	0.919	0.913	0.838	0.937
T4	0.941	0.943	0.859	0.834	0.979	0.906	0.922	0.851	0.941
T5	0.970	0.967	0.866	0.810	0.971	0.897	0.892	0.816	0.938
T6	0.948	0.935	0.862	0.777	0.968	0.915	0.919	0.855	0.941
T7	0.948	0.952	0.856	0.783	0.959	0.906	0.882	0.825	0.908
T8	0.945	0.943	0.874	0.782	0.965	0.878	0.885	0.826	0.938
T9	0.952	0.949	0.843	0.804	0.968	0.865	0.883	0.798	0.910
T10	0.945	0.914	0.817	0.805	0.947	0.896	0.894	0.821	0.880
Ave.	0.950	0.941	0.854	0.797	0.966	0.901	0.898	0.831	0.925
Average sensitivity from all slices:0.896									
Specificity	S1	S2	S3	S4	S5	S6	S7	S8	S9
T1	0.809	0.743	0.787	0.808	0.720	0.769	0.715	0.854	0.847
T2	0.813	0.741	0.790	0.804	0.721	0.770	0.722	0.852	0.845
T3	0.813	0.736	0.786	0.799	0.730	0.766	0.714	0.850	0.842
T4	0.828	0.760	0.822	0.812	0.729	0.776	0.724	0.860	0.852
T5	0.804	0.732	0.785	0.788	0.736	0.789	0.731	0.869	0.858
T6	0.820	0.749	0.801	0.813	0.748	0.746	0.691	0.844	0.843
T7	0.817	0.744	0.795	0.807	0.726	0.775	0.730	0.860	0.847
T8	0.817	0.762	0.805	0.827	0.750	0.797	0.742	0.856	0.854
T9	0.821	0.753	0.798	0.820	0.740	0.786	0.732	0.852	0.852
T10	0.770	0.715	0.705	0.745	0.739	0.771	0.728	0.849	0.834
Ave.	0.811	0.743	0.787	0.802	0.734	0.774	0.723	0.855	0.847
Average specificity from all slices:0.786									

Table 2. Segmentation accuracy for lipid and fibrous tissue using M1 and M2. Sen: Sensitivity; Spe: Specificity; Acc: Accuracy.

	M 1			M 2		
Slice#	Sen	Spe	Acc	Sen	Spe	Acc
1	0.950	0.811	0.834	0.829	0.789	0.795
2	0.941	0.743	0.771	0.792	0.714	0.725
3	0.854	0.787	0.799	0.720	0.761	0.754
4	0.797	0.802	0.800	0.648	0.785	0.743
5	0.966	0.734	0.743	0.900	0.685	0.693
6	0.901	0.774	0.782	0.701	0.762	0.758
7	0.898	0.723	0.740	0.787	0.717	0.724
8	0.831	0.855	0.852	0.646	0.844	0.820
9	0.925	0.847	0.854	0.817	0.835	0.834
Ave.	0.896	0.786	0.797	0.760	0.766	0.761

3.2 Cap thickness

For all 9 co-registered OCT/VH-IVUS images, five different segmentation methods (manual segmentation (denoted as Ma), M1, M2, IVUS50 and IVUS180) were applied to detect the lipid contours and lumen borders. The cap thickness between lumen and a particular lipid was calculated for many locations on the lumen. The average value and minimum over the cap is recorded in Table 3 as mean cap thickness and min cap thickness. Using manual segmentation as standard, M1 and M2 generally gave better results than IVUS50 and IVUS180. The average of mean cap thickness (9 slices, unit: mm) from 5 groups were 0.561, 0.470, 0.463, 0.128, and 0.204, respectively. Average values from M1 and M2 were about same value. The average values of M1, M2, IVUS50 and IVUS180 were 16.3%, 17.4%, 77.2% and 63.6% less than Ma, respectively. Average of minimum cap thickness (9 slices) from 5 groups were 0.390, 0.288, 0.282, 0.040, and 0.165, respectively. The average min values of M1, M2, IVUS50 and IVUS180 were 26.0%, 27.5%, 89.6% and 57.6% less than Ma, respectively.

Table 3. Mean cap thickness and minimum cap thickness for 9 slices from five groups.

Mean Cap Thickness(mm)									
Slice#	Ma	M1	error	M2	error	IVUS 50	error	IVUS 180	error
1	0.597	0.484	18.9%	0.459	23.1%	0.166	72.2%	0.239	60.1%
2	0.683	0.483	29.2%	0.446	34.8%	0.123	82%	0.208	69.5%
3	0.765	0.492	35.7%	0.478	37.5%	0.094	87.8%	0.196	74.4%
4	0.337	0.383	13.5%	0.350	3.9%	0.120	64.5%	0.203	39.8%
5	0.575	0.399	30.6%	0.455	20.9%	0.173	69.9%	0.216	62.5%
6	0.491	0.484	1.3%	0.459	6.5%	0.087	82.3%	0.178	63.6%
7	0.477	0.412	13.6%	0.412	13.7%	0.139	70.9%	0.209	56.2%
8	0.539	0.572	6.2%	0.549	1.9%	0.144	73.3%	0.210	61.1%
9	0.584	0.515	11.9%	0.561	4.7%	0.103	82.3%	0.181	69%
Ave.	0.561	0.470	16.3%	0.463	17.4%	0.128	77.2%	0.204	63.6%
Min Cap Thickness(mm)									
1	0.497	0.308	38%	0.314	36.9%	0.050	89.8%	0.172	65.4%
2	0.429	0.330	23.1%	0.225	47.6%	0.042	90.2%	0.165	61.5%
3	0.539	0.285	47.2%	0.285	47.2%	0.035	93.5%	0.170	68.5%
4	0.158	0.150	5.0%	0.163	3.0%	0.033	78.9%	0.159	0.5%
5	0.331	0.163	50.8%	0.227	31.6%	0.042	87.4%	0.165	50.3%
6	0.326	0.285	12.7%	0.274	16.0%	0.039	88.1%	0.162	50.5%
7	0.392	0.338	13.7%	0.295	24.7%	0.043	89.2%	0.167	57.3%
8	0.445	0.413	7.3%	0.427	4.0%	0.050	88.7%	0.164	63.1%
9	0.390	0.324	16.8%	0.333	14.5%	0.030	92.4%	0.163	58.2%
Ave.	0.390	0.288	26.0%	0.282	27.5%	0.040	89.6%	0.165	57.6%

3.3 Point-point cap thickness

The cap thickness were compared by point to point for from five segmentation methods. Some points from IVUS contours were matched one-by-one by sharing the same location with some points from OCT contours. Slice 4 had the minimum of min cap thickness less than 180μm

according to the manual segmentation (0.158 mm), and the slice 1 had the maximum of min cap thickness in 9 slices. So slice 1 and slice 4 were selected to match points for comparing the point-point cap thickness. The matching points were showed in Figure 6. And the cap thickness of matched points were given in Table 4 and Table 5. Point 1-Point 4 from slice 4 were close to 180 μm, and the cap thickness difference between M1 and M2 were less than 14%. The cap thickness values of IVUS180 were overestimated about 10% than the value from OCT. The cap thickness values from IVUS50 were underestimated about 70% than the cap thickness from OCT. Point 10-14 from slice 4 were about 300μm. The cap thickness of IVUS50 and IVUS180 were underestimated by about 80% and 50%. The cap thickness values of two segmentation methods (IVUS50 and IVUS180) were largely determined by the previously educated guesses.

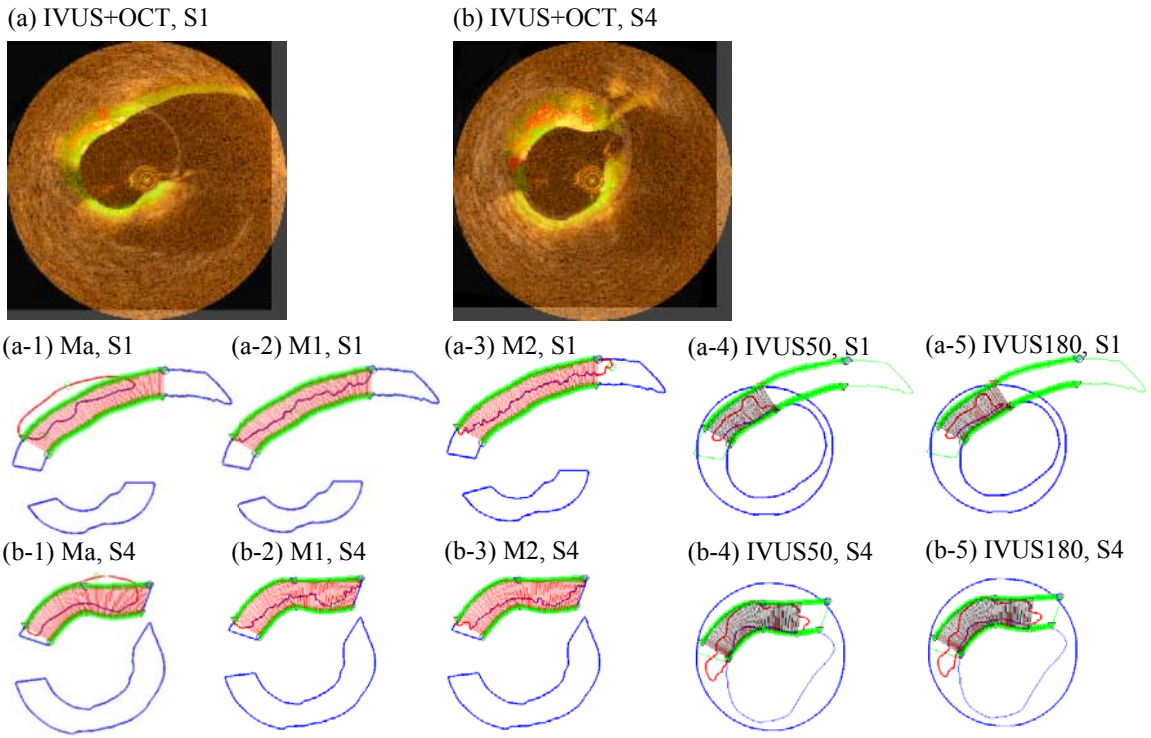

Figure 6. The point-point cap thickness in slice 1 and slice 4. (a) S1 OCT image overlaid with S1 IVUS image. (b) S4 OCT image overlaid with S4 IVUS image. (a-1) cap thickness from Manual segmentation in slice 1. (a-2) cap thickness from M1 in slice 1. (a-3) cap thickness from M2 in slice 1. (a-4) cap thickness from IVUS50 in slice 1. (a-5) cap thickness from IVUS180 in slice 1. (b-*) is in slice 4, and similar to (a-*).

Table 4. Point- point cap thickness in slice 1 from five groups.

Point to Point Cap thickness(mm)					
Slice 1 point	Ma	M1	M2	IVUS50	IVUS180
1	0.642	0.538	0.539	0.057	0.171
2	0.579	0.542	0.551	0.054	0.183
3	0.543	0.443	0.460	0.054	0.171
4	0.522	0.405	0.428	0.054	0.176
5	0.507	0.398	0.376	0.053	0.179
6	0.500	0.411	0.384	0.057	0.171
7	0.497	0.422	0.387	0.053	0.175
8	0.501	0.416	0.351	0.054	0.172
9	0.513	0.434	0.350	0.049	0.178
10	0.544	0.456	0.467	0.052	0.180
11	0.591	0.434	0.406	0.053	0.186
12	0.644	0.440	0.346	0.076	0.191
13	0.675	0.442	0.328	0.082	0.198
14	0.681	0.395	0.321	0.105	0.195
15	0.669	0.400	0.352	0.147	0.191
16	0.650	0.411	0.314	0.149	0.197
17	0.623	0.405	0.347	0.159	0.186
18	0.596	0.451	0.364	0.202	0.203
19	0.572	0.497	0.368	0.224	0.226
20	0.552	0.507	0.532	0.242	0.244
21	0.536	0.485	0.472	0.253	0.254
22	0.524	0.524	0.415	0.285	0.287
23	0.515	0.537	0.571	0.296	0.296
24	0.515	0.526	0.608	0.310	0.312
25	0.528	0.535	0.631	0.326	0.327
26	0.568	0.563	0.565	0.339	0.339
27	0.642	0.591	0.540	0.345	0.345

Table 5. Point- point cap thickness in slice 4 from five groups.

Point to Point Cap thickness(mm)					
Slice 4 point	Ma	M1	M2	IVUS50	IVUS180
1	0.158	0.150	0.165	0.052	0.180
2	0.159	0.171	0.170	0.048	0.179
3	0.164	0.189	0.173	0.045	0.172
4	0.172	0.191	0.202	0.044	0.169
5	0.182	0.192	0.223	0.038	0.166
6	0.190	0.246	0.204	0.038	0.167
7	0.303	0.314	0.290	0.050	0.173
8	0.307	0.300	0.289	0.055	0.178
9	0.312	0.321	0.279	0.051	0.171
10	0.319	0.430	0.283	0.052	0.173
11	0.329	0.427	0.298	0.056	0.177
12	0.337	0.320	0.311	0.060	0.179
13	0.340	0.326	0.311	0.076	0.181
14	0.346	0.340	0.296	0.117	0.180
15	0.350	0.340	0.346	0.284	0.284
16	0.351	0.337	0.369	0.283	0.283
17	0.355	0.321	0.361	0.292	0.292
18	0.359	0.344	0.353	0.305	0.305
19	0.391	0.396	0.388	0.330	0.330
20	0.403	0.387	0.326	0.285	0.285
21	0.416	0.382	0.347	0.239	0.239
22	0.428	0.374	0.375	0.216	0.216

4. Discussion

4.1 Significance of OCT images for cap thickness

Imaging resolution has been a major limitation for vulnerable plaque research (and other areas in a broader sense) since the introduction of medical imaging. With image resolutions at 150 μm (IVUS) – 300 μm (MRI) or even worse, and plaque vessel wall thickness changes were normally under 200 μm, and "vulnerable plaque" cap thickness threshold value defined as 65 μm, many published results were educated guesses by segmentation software. Possessing the capability of detecting thin fibrous cap, OCT is able to provide more accurate cap thickness information to promote both the morphological and mechanical analyses in vulnerable plaque research.

4.2 Prediction for cap thickness

Using manual segmentation as standard, IVUS50 and IVUS180 would underestimate the real cap thickness. Particularly, IVUS50 demonstrated an overall worse ability in estimating the cap thickness. Regarding to some particular thickness values, IVUS180 provided relatively accurate cap thickness measurement when the cap thickness is about 180 μm. While IVUS50 and IVUS180 showed no ability in capturing reasonable cap thickness.

Among the different segmentation methods, predictions from LS-SVM (M1 and M2) showed higher agreements with manual segmentation in measuring mean cap thickness, comparing to IVUS50 and IVUS180. The relative error between M1/M2 and manual segmentation is less than 17.2% for mean cap thickness, and less than 26.4%, if we look at the minimum cap thickness.

4.3 Limitations

One major limitation of this study is lack of histology data as the golden standard. Manual segmentation results based on IVUS and OCT images were considered as the alternative to the golden standard. Another limitation is the small sample size of OCT image studied. Large-scale studies with more OCT image are needed to validate and improve the significance of prediction method.

Funding:

This research was supported in part by NIH grant R01 EB004759 and a Jiangsu Province Science and Technology Agency grant BE2016785.

Conflict of Interest:

There are no conflicts of interest in this study.

References

1. Virmani R, Kolodgie, FD, Burke AP, Farb A, Schwartz SM. Lessons from sudden coronary death: a comprehensive morphological classification scheme for atherosclerotic lesions. *Arteriosclerosis Thrombosis, and Vascular Biology* 2000; 20(5), 1262-1275.
2. Finn AV, Nakano M, Narula J, Kolodgie FD, Virmani R. Concept of vulnerable/unstable plaque. *Arteriosclerosis, thrombosis, and vascular biology* 2010; 30(7):1282-92.
3. Tang D, Kamm RD, Yang C, Zheng J, Canton G, Bach R, Huang X, Hatsukami TS, Zhu J, Ma G, Maehara A. Image-based modeling for better understanding and assessment of atherosclerotic plaque progression and vulnerability: Data, modeling, validation, uncertainty and predictions. *Journal of biomechanics* 2014; 47(4):834-46.
4. Wang L, Wu Z, Yang C, Zheng J, Bach R, Muccigrosso D, Billiar K, Maehara A, Mintz GS, Tang D. IVUS-based FSI models for human coronary plaque progression study: components, correlation and predictive analysis. *Annals of biomedical engineering* 2015; 43(1):107-21.
5. Kubo T, Maehara A, Mintz GS, et al. The dynamic nature of coronary artery lesion morphology assessed by serial virtual histology intravascular ultrasound tissue characterization. *Journal of the American College of Cardiology* 2010; 55(15): 1590-1597.
6. Jang I K, Bouma B E, Kang D H, et al. Visualization of coronary atherosclerotic plaques in patients using optical coherence tomography: comparison with intravascular ultrasound. *Journal of the American College of Cardiology* 2002; 39(4): 604-609.
7. Tearney GJ, Regar E, Akasaka T, et al. Consensus standards for acquisition, measurement, and reporting of intravascular optical coherence tomography studies. *Journal of the American College of Cardiology* 2012; 59(12): 1058-1072.
8. Bezerra HG, Costa MA, Guagliumi G, et al. Intracoronary optical coherence tomography: a comprehensive review: clinical and research applications. *JACC: Cardiovascular Interventions* 2009; 2(11): 1035-1046.
9. Jang IK, Tearney GJ, MacNeill B, et al. In vivo characterization of coronary atherosclerotic plaque by use of optical coherence tomography. *Circulation* 2005; 111(12): 1551-1555.
10. Yabushita H, Bouma BE, Houser SL, et al. Characterization of human atherosclerosis by optical coherence tomography. *Circulation* 2002; 106(13): 1640-1645.
11. Räber L, Heo J H, Radu M D, et al. Offline fusion of co-registered intravascular ultrasound and frequency domain optical coherence tomography images for the analysis of human atherosclerotic plaques. *EuroIntervention* 2012; 8(1): 98-108.

12. Wang Z, Kyono H, Bezerra HG, et al. Semiautomatic segmentation and quantification of calcified plaques in intracoronary optical coherence tomography images. *Journal of biomedical optics* 2010; 15(6): 061711-061711-10.
13. Wang Z, Chamie D, Bezerra HG, et al. Volumetric quantification of fibrous caps using intravascular optical coherence tomography. *Biomedical optics express* 2012; 3(6): 1413-1426.
14. Xu C, Schmitt JM, Carlier SG, et al. Characterization of atherosclerosis plaques by measuring both backscattering and attenuation coefficients in optical coherence tomography. *Journal of biomedical optics* 2008; 13(3): 034003-034003-8.
15. Van Soest G, Regar E, KoljenoviÄ S, et al. Atherosclerotic tissue characterization in vivo by optical coherence tomography attenuation imaging. *Journal of biomedical optics* 2010; 15(1): 011105-011105-9.
16. Athanasiou LS, Bourantas CV, Rigas G, et al. Methodology for fully automated segmentation and plaque characterization in intracoronary optical coherence tomography images. *Journal of biomedical optics* 2014; 19(2): 026009-026009.
17. Shalev R, Prabhu D, Tanaka K, et al. Intravascular optical coherence tomography image analysis method. Biomedical Engineering Conference (NEBEC), 2015 41st Annual Northeast. IEEE, 2015: 1-2.
18. Gargesha M, Shalev R, Prabhu D, et al. Parameter estimation of atherosclerotic tissue optical properties from three-dimensional intravascular optical coherence tomography. *Journal of medical imaging* 2015; 2(1): 016001-016001
19. Ughi GJ, Adriaenssens T, Sinnaeve P, et al. Automated tissue characterization of in vivo atherosclerotic plaques by intravascular optical coherence tomography images. *Biomedical optics express* 2013; 4(7): 1014-1030.
20. Tsantis S, Kagadis G C, Katsanos K, et al. Automatic vessel lumen segmentation and stent strut detection in intravascular optical coherence tomography. *Medical physics* 2012; 39(1): 503-513.
21. Haralick RM, Shanmugam K. Textural features for image classification. *IEEE Transactions on systems, man, and cybernetics* 1973; 3(6): 610-621.
22. Suykens J A K, Vandewalle J. Least squares support vector machine classifiers. *Neural processing letters* 1999; 9(3): 293-300.
23. Suykens J A K, Van Gestel T, De Brabanter J. Least squares support vector machines. *World Scientific* 2002.